

Article

New Insights into Sensitization Mechanism of the Doped Ce (IV) into Strontium Titanate

Taiping Xie ^{1,2,*} , Yuan Wang ^{3,4}, Chenglun Liu ^{2,4} and Longjun Xu ^{2,*}

¹ Chongqing Key Laboratory of Extraordinary Bond Engineering and Advanced Materials Technology (EBEAM), Yangtze Normal University, Chongqing 408100, China

² State Key Laboratory of Coal Mine Disaster Dynamics and Control, Chongqing University, Chongqing 400044, China; xlclj@cqu.edu.cn

³ Environmental Monitoring Center Station of Suining City, Suining 629000, China; wangyuan@163.com

⁴ College of Chemistry and Chemical Engineering, Chongqing University, Chongqing 400044, China

* Correspondence: deartaiping@163.com (T.X.); xulj@cqu.edu.cn (L.X.)

Received: 17 March 2018; Accepted: 18 April 2018; Published: 23 April 2018



Abstract: SrTiO₃ and Ce⁴⁺ doped SrTiO₃ were synthesized by a modified sol–gel process. The optimization synthesis parameters were obtained by a series of single factor experiments. Interesting phenomena are observable in Ce⁴⁺ doped SrTiO₃ systems. Sr²⁺ in SrTiO₃ system was replaced by Ce⁴⁺, which reduced the surface segregation of Ti⁴⁺, ameliorated agglomeration, increased specific surface area more than four times compared with pure SrTiO₃, and enhanced quantum efficiency for SrTiO₃. Results showed that Ce⁴⁺ doping increased the physical adsorption of H₂O and adsorbed oxygen on the surface of SrTiO₃, which produced additional catalytic active centers. Electrons on the 4f energy level for Ce⁴⁺ produced new energy states in the band gap of SrTiO₃, which not only realized the use of visible light but also led to an easier separation between the photogenerated electrons and holes. Ce⁴⁺ repeatedly captured photoelectrons to produce Ce³⁺, which inhibited the recombination between photogenerated electrons and holes as well as prolonged their lifetime; it also enhanced quantum efficiency for SrTiO₃. The methylene blue (MB) degradation efficiency reached 98.7% using 3 mol % Ce⁴⁺ doped SrTiO₃ as a photocatalyst, indicating highly photocatalytic activity.

Keywords: strontium titanate; Ce(IV); doping modification; photocatalyst

1. Introduction

SrTiO₃ is a good stability photocatalyst, possessing a relative narrow band gap. It is a promising function material which has been widely used in water decomposition to produce hydrogen, degradation of organic pollutants, and photochemical cells fields [1].

The excitation wavelength for SrTiO₃ is 387 nm, which places it in UV light range. Visible light range is from 400 to 700 nm, occupying 50% of the solar light spectrum [2]. Therefore, an extension of the absorption light range of SrTiO₃ into visible light may promote additional practical applications.

Many researchers have successfully prepared nano-structured SrTiO₃ by various synthesis methods. However, these methods have several disadvantages; for example, low yield, high pollution, high cost, and complicated preparation processes. Accordingly, an exploration of environmentally friendly and low cost synthesis approaches for nano-SrTiO₃ is important.

The function of doped ions is to capture and release photogenerated carriers quickly [3], thereby controlling the diffusion of photogenerated carriers in the catalyst particles, increasing the lifetime of photogenerated carriers, and improving the photocatalytic performance of a single-component photocatalyst.

The unique electronic structure of rare earth elements provides several thermodynamic and kinetic advantages [4]. Such elements have variable valence oxidation states under certain conditions. In the photocatalytic reaction process, variable valence can effectively transfer photogenerated electrons to prolong the time needed for the effective separation between photogenerated electrons and holes. Concurrently, the amount of rare earth elements can change the band gap of a single-component photocatalyst and expand its light absorption range.

The rare earth element cerium (Ce) can produce multiple electronic configurations and absorb visible light. It is the ideal application by which to dope elements for photocatalyst modification. Previous research has suggested [5–9] electron transfer between Ce^{4+} and Ce^{3+} may enhance photocatalytic activity of ZnO, Al_2O_3 , and TiO_2 as a result of the Ce dopant capturing the photogenerated electrons and suppressing the recombination of electron–hole pairs. In addition, an appropriate amount of doped Ce may enhance the property of corrosion resistance to ensure reuse for the modified products. Nevertheless, modification research for SrTiO_3 by doping Ce^{4+} has not yet been reported.

Here, we report an environmentally friendly and low cost synthesis method with a simple preparation process in which Ce^{4+} doped SrTiO_3 in situ synthesis was carried out to modify SrTiO_3 .

2. Experimental Procedures

All reagents were of analytical grade purity and used directly without further purification except that of SrCO_3 . The water used in all experiment processes was deionized water.

2.1. Preparation of Pure SrTiO_3

SrCO_3 was prepared according to the sol–gel method. A transparent mixed solution (marked A), including 1.47 g SrCO_3 and tartaric acid with different ratios, was prepared by mixing and stirring at 60 °C for 10 min. Subsequently, 3.4 mL butyl titanate was added to the (A) solution under stirring conditions at 80 °C to form a yellow homogeneous sol. The prepared homogeneous sol was dried at 90 °C for 10 h to obtain dry gel. The resultant product was obtained by calcining the dry gel at 800 °C for 2 h.

2.2. Preparation of Ce-Doped SrTiO_3

Ce-doped SrTiO_3 was prepared according to the in situ sol–gel method. Under the optimum conditions of SrTiO_3 preparation, ammonium ceric nitrate was added to the (A) solution. The addition amount (x) was 1 mol %~4 mol %. Other processes were not changed. It could be observed from the resultant product that an increase in the amount of ammonium ceric nitrate doped corresponded to a gradually deepening orange color in the product.

2.3. Materials Characterizations

Fourier transform infrared spectroscopy (FTIR) spectra of samples were recorded on an FTIR (Perkin-Elmersystem 2000, Akron, OH, USA) spectrometer using KBr powder-pressed pellets. Phase identification via X-ray diffraction (XRD) was conducted on an X-ray diffractometer (Shimadzu, XRD-6000, Kyoto, Japan) using $\text{Cu K}\alpha$ irradiation at a scanning rate of $4^\circ \cdot \text{min}^{-1}$ with the 2θ range of 20° – 70° . X-ray photoelectron spectroscopy (XPS) measurements were carried out on an XPS-XSAM800 (Kratos, Manchester, UK) spectrometer with an achromatic $\text{Al K}\alpha$ X-ray source and an analytical chamber with a base pressure of 2×10^{-7} Pa. The X-ray gun was operated at 180W (12 kV, 15 mA). The Brunauer-Emmett-Teller (BET) special surface area was determined through N_2 adsorption at 77 K using an adsorption instrument (ASAP-2020, Micromeritics, Norcross, GA, USA). The samples' morphologies and microstructures were observed via a scanning electron microscopy (SEM, FEI, F50, ZEISS, Oberkochen, Germany) The UV-vis diffuse reflectance spectra (DRS) of samples were measured using a UV-vis spectrophotometer (TU1901, Beijing Purkinje, Beijing, China). BaSO_4 was used as a reflectance standard.

2.4. Photocatalytic Activity Tests

100 mL of methylene blue (MB) aqueous solution with a given concentration and its corresponding photocatalyst dosage of 1 g/L were added into a quartz container and stirred for 1 h in the dark to reach the adsorption-desorption equilibrium. A 500 W Xe lamp equipped with UV cut-off filter was used as the visible light source ($\lambda \geq 420$ nm). At the given irradiation time intervals, a series of the reaction solution was sampled and the absorption was measured with the UV-vis spectrophotometer (TU1901, Beijing Purkinje, Beijing, China).

2.4.1. Effect of Initial Concentration of Methylene Blue on Photocatalytic Activity

According to the literature, initial concentration had a significant influence on the photocatalytic activity. A greater concentration of methylene blue produced a deeper color, which significantly affected the absorption of light irradiation for photocatalysts. Too low of a methylene blue concentration cannot fully reflect the photocatalytic activity. Therefore, to completely reveal photocatalytic activity of SrTiO₃, a better initial concentration should be chosen via single factor experiment.

Here, we prepared a series of MB solutions with different concentrations (20 mg/L, 50 mg/L, 100 mg/L, 150 mg/L, and 200 mg/L). The degradation rate after 2 h reaction was tested using pure SrTiO₃ and Ce-doped SrTiO₃ as photocatalyst.

2.4.2. Effect of Ce Doping Amount on Photocatalytic Activity

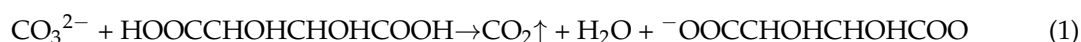
In order to investigate the effect of the Ce doping amount on the photocatalytic activity of SrTiO₃, the photocatalysis mechanism was discussed and comparative experiments were performed. Four varieties of SrTiO₃ with Ce content of 1 mol %–4 mol % were measured using photocatalytic reaction.

3. Results and Discussion

3.1. Optimization of Synthesis Conditions

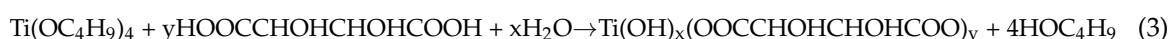
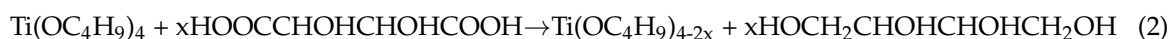
3.1.1. Effect of Tartaric Acid Dosage

In this synthesis process, tartaric acid was used as the solvent of SrCO₃ and also as the complexing agent of tetrabutyl titanate. The following reaction occurred as a solvent for SrCO₃:



The formation of homogeneous sol-gel via the complexation reaction between butyl titanate and tartaric acid was divided into two steps:

First, the stable organic complex of Ti⁴⁺ was formed by mixing butyl titanate with tartaric acid under stirring condition.



Second, Ti⁴⁺ complexes could create a network structure in the sol-gel system by cross-linking action. In this process, Sr²⁺ ions were uniformly distributed in the sol-gel system by electrostatic action.

It can be seen from the reaction process that the amount of tartaric acid could not only dissolve SrCO₃ but also ensure the complete complexation of Ti⁴⁺ with tartaric acid in order to obtain a stable organic complex including Ti⁴⁺.

When the amount of organic complexing agent was too small, the reaction system produced precipitation phenomenon; this resulted from the minimal presence of the complexing agent, which did not fully react with the metal ion. Accordingly, metal salt precipitation and crystallization made the formation of a clear and transparent sol more difficult.

In addition, tartaric acid also acts as a stabilizing agent in the formation of network-structured sol–gels through the cross-linking reaction between tartaric acid and Ti^{4+} . In the sol–gel method process, the entire reaction system has no active group for polycondensation reaction.

The reaction between Ti^{4+} complex molecules was achieved only through the formation of hydrogen bonds from water molecules instead of polycondensation reaction. However, the hydrogen bond was not stable and easily disconnected. Accordingly, this kind of gel with cross-linking of hydrogen bonds easily absorbed water and subsequently was moisturized in the atmosphere. When the deliquescence gel was sintered at a high temperature, an undesired agglomeration phenomenon was observed in the resultant product. Fortunately, the tartaric acid contained numerous hydroxyl groups which could replace the hydrogen bonds via the crosslinking reaction process. Thus, a more stable, uniform transparent gel was formed.

Therefore, in the preparation process, the amount of tartaric acid must meet the needs of the solvent for $SrCO_3$, the complexing agent of butyl titanate, and the stabilizer of the entire reaction system. However, an excessive amount of complexing agent in the preparation process might incur high costs.

To adjust the mole ratio of Sr^{2+} and tartaric acid to 2:1–1:5 in the preparation process of $SrTiO_3$, the optimal dosage of tartaric acid was chosen by observing sol transparency and powder agglomeration after sintering, calculating relative crystallinity (The relative crystallinity can be obtained by processing XRD data of the sample.), and photocatalytic activity of the products. Table 1 lists the experimental phenomena and relative crystallinity of $SrTiO_3$ in the system with different molar ratios of Sr^{2+} and tartaric acid (2:1–1:5).

Table 1. Experimental phenomena and relative crystallinity of $SrTiO_3$ in the system with different molar ratios of Sr^{2+} and tartaric acid.

Sample Number	$n_{(Sr^{2+})}/n_{(tartaric\ acid)}$	Sol State	Relative Crystallinity (%)
1	2:1	white precipitation	23
2	1:1	white precipitation	27
3	1:2	transparent	78
4	1:3	transparent	85
5	1:4	transparent	89
6	1:5	transparent	89

As seen in Table 1, the molar ratio of Sr^{2+} and tartaric acid was higher than 1:1, the white precipitation was observed, and the relative crystallinity of the product was low. These phenomena indicated that tartaric acid added in the system was not sufficient to completely generate complexation reaction with Ti^{4+} .

To further investigate the influence of tartaric acid dosage on the photocatalytic activity of $SrTiO_3$, the samples were used in a photocatalytic activity test, and the experimental results are shown in Figure 1. It can be seen that the photocatalytic activity of $SrTiO_3$ for methylene blue was greatly affected by the amount of tartaric acid. When the molar ratio of Sr^{2+} and tartaric acid was less than 1:4, the photocatalytic activity was highest. In contrast, when the molar ratio of Sr^{2+} and tartaric acid was 1:5, the photocatalytic activity was lower. Therefore, the optimum molar ratio of Sr^{2+} and tartaric acid was 1:4.

Concurrently, Table 1 and Figure 1 also demonstrate that the degradation rate of methylene blue was enhanced with the increase in the relative crystallinity of the as-prepared $SrTiO_3$. This provided a theoretical basis for the modification of $SrTiO_3$.

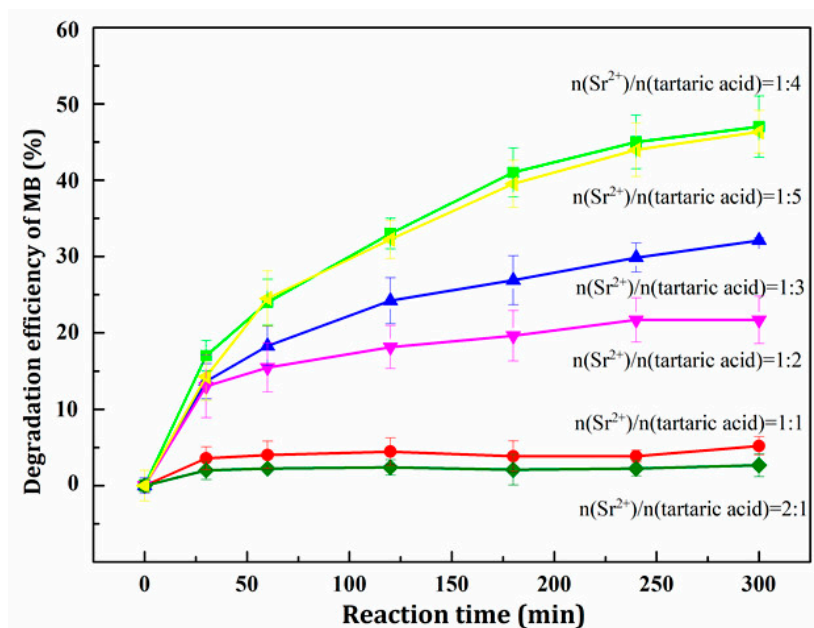


Figure 1. Effect of different dosage of tartaric acid on degradation efficiency of MB.

3.1.2. Effect of Distilled Water Amount

The dissolution of SrCO₃ and tartaric acid, the multistage ionization of tartaric acid, and the formation of sol–gel by the strontium titanate precursor all occurred in aqueous solution. Therefore, the amount of distilled water affected the preparation process of SrTiO₃. When the water content in the solution was insufficient, the solution generated precipitation phenomenon due to low dissolution ability to SrCO₃ and tartaric acid. Meanwhile, tartaric acid belonged to H₂A-type acid. Accordingly, there was secondary ionization equilibrium in the solution.



Obviously, the amount of distilled water affected the pH value of the solution. The ionization degree of tartaric acid was different in solutions with various pH values. On the one hand, the insufficient amount of distilled water restrained the secondary ionization of tartaric acid, which led to difficulty in obtaining clear sol. On the other hand, although additional distilled water helped to dissolve SrCO₃ and tartaric acid, too much water reduced the collision probability of Ti⁴⁺ and tartrate ions in solution, which brought about the incomplete complexation reaction.

At the same time, excessive water extended the drying time and increased the cost. Only when the water content was appropriate did the following reactions occur: (a) the SrCO₃ and tartaric acid fully dissolved, (b) the tartaric acid was completely ionized, and (c) complexation reaction occurred completely. Only when such conditions were met could a clear and transparent homogeneous sol be obtained.

To determine the optimum amount of distilled water (5–25 mL) factors such as the observation of sol transparency, powder agglomeration after sintering, calculation of relative crystallinity, and photocatalytic activity of products were considered.

Table 2 provides the experimental phenomena for SrTiO₃ and the relative crystallinity determined by adjusting the amount of distilled water. It can be seen from Table 2 that when the amount of distilled water was less than 10 mL, the solubility of SrCO₃ and tartaric acid was relatively weak, the secondary ionization of tartaric acid was inhibited, and the white precipitate in the sol system could be observed. When the amount of distilled water was 15 mL, the relative crystallinity of the product was still not

high despite a transparent sol. When the amount of distilled water was 25 mL, a white precipitate appeared in the sol system, indicating that the distilled water was excessive, that the reaction in the system was incomplete, and that the drying time would be lengthened.

Table 2. Experimental phenomena and relative crystallization of SrTiO₃ prepared with different amounts of water.

Sample Number	H ₂ O (mL)	Sol State	Drying Time (h)	Relative Crystallinity (%)
1	5	white precipitation	5	13
2	10	white precipitation	6	20
3	15	transparent	8	80
4	20	transparent	10	89
5	25	white precipitation	15	89

To investigate the influence of the amount of distilled water on the photocatalytic activity of the as-prepared SrTiO₃, the samples were used for the photocatalytic activity test. Results are shown in Figure 2. It can be seen that when the amount of distilled water was 20 mL, methylene blue had the highest degradation rate. Therefore, the optimum amount of distilled water was found to be 20 mL.

In addition, Table 2 and Figure 2 demonstrate that the higher the crystallinity of the catalyst, the higher the rate of MB degradation.

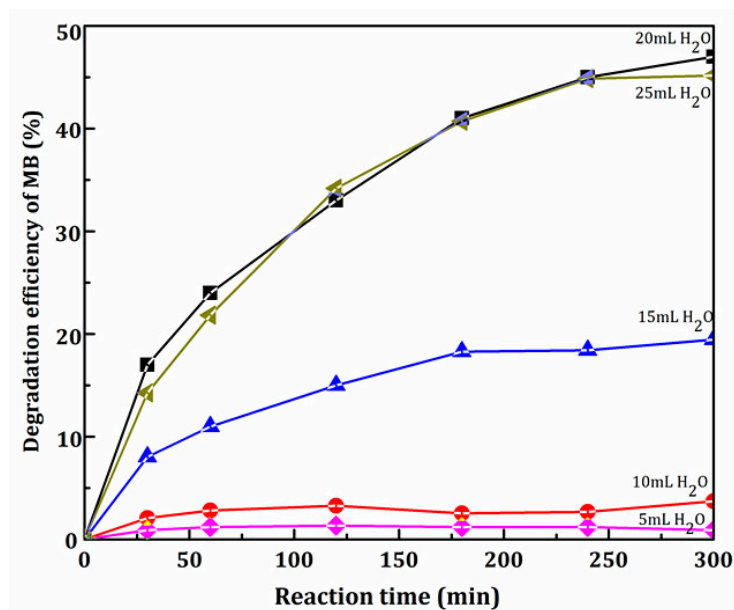


Figure 2. Effect of different dosage of water on MB degradation.

3.2. XRD, IR, and SEM Analysis of SrTiO₃

In the preparation process of SrTiO₃, the molar ratio of Sr²⁺ to tartaric acid was less than 1:4 and the amount of distilled water was 20 mL. The as-prepared SrTiO₃ was characterized by XRD, IR, BET, and SEM. Figure 3 shows the XRD pattern of SrTiO₃ prepared under optimum conditions. Compared with the standard card, diffraction peaks at $2\theta = 23.0^\circ, 32.4^\circ, 40.4^\circ, 57.8^\circ, 67.8^\circ, 77.2^\circ,$ and 79.9° belonged to the 100, 110, 111, 200, 211, 220, and 310 of the crystal phase of SrTiO₃ [10–12], respectively. It can be seen that the prepared SrTiO₃ had a good crystal form and a high diffraction peak intensity. The average particle size of SrTiO₃ was 20.8 nm calculated by the Debye-Scherrer formula, which reached nanometer level. The crystallinity of SrTiO₃ was 89%. The BET test results indicated that the specific surface area was 11.8 m²/g. The specific surface area was relatively small,

which was not conducive to improving photocatalytic activity. Therefore, subsequent experiments to modify SrTiO₃ to improve its crystallinity and to increase its specific surface area were conducted.

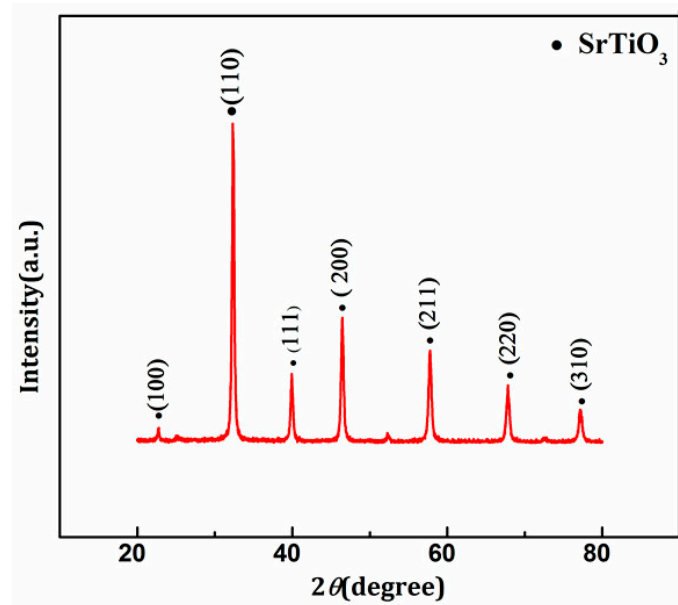


Figure 3. XRD pattern of pure SrTiO₃.

Figure 4 displays the FTIR spectrum of SrTiO₃. The absorption peaks at 3420 cm⁻¹ and 1629 cm⁻¹ originated from hydroxyl vibration [3]. It is speculated that the hydroxyl group was derived from the adsorption water on the surface of the sample. The absorption peak at 557 cm⁻¹ belonged to the characteristic stretching vibration of the Sr-Ti-O bond [11], which confirmed SrTiO₃ was prepared successfully.

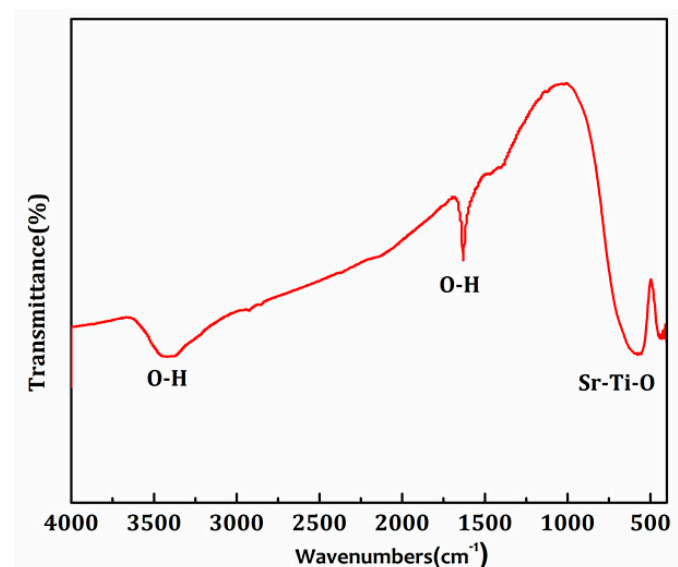


Figure 4. FTIR spectra of pure SrTiO₃.

It can be seen from Figure 5 that pure SrTiO₃ particles were spherical. Agglomeration was formed in part as a result of the volatilization or decomposition of organic compounds during the roasting process.

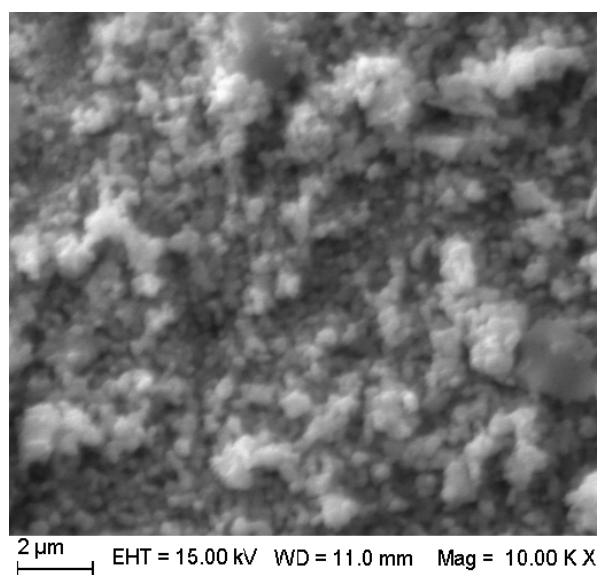


Figure 5. SEM images of pure SrTiO₃.

3.3. XRD, BET, IR, XPS, and SEM Analysis of Ce⁴⁺ Doped SrTiO₃

From Figure 6a, the diffraction peaks of SrTiO₃ appear in each of the patterns. The XRD diffraction peaks of Ce⁴⁺ doped SrTiO₃ from 1 mol % to 4 mol % were in good agreement with that of pure SrTiO₃, indicating that the incorporation of Ce⁴⁺ could not change the crystal structure of SrTiO₃. There was no Ce⁴⁺ independent characteristic diffraction peak in the spectra, demonstrating that Ce⁴⁺ was highly dispersed into SrTiO₃, even into the crystal lattice of SrTiO₃. Figure 6b demonstrates that, with the increase of the doping amount of Ce⁴⁺, the diffraction peak of crystal plane of SrTiO₃ (110) gradually broadened and shifted to a higher 2θ direction, further indicating that Ce⁴⁺ entered the framework of SrTiO₃ [5–7] and substituted Sr²⁺ in SrTiO₃ system. The ionic radius for Ti⁴⁺, Ce⁴⁺, and Sr²⁺ showed a higher order of increase from 68 to 113 pm, namely, $r_{Ti^{4+}}$ (68 pm) < $r_{Ce^{4+}}$ (92 pm) < $r_{Sr^{2+}}$ (113 pm). A replacement of Ce⁴⁺ for Sr²⁺ would reduce the lattice parameter (d) according to the Bragg law ($n\lambda = 2d\sin\theta$, $n = 1$). The decrease in d values would cause the shift of diffraction peaks to high 2θ direction. The broadening of the manifest diffraction peak indicated that the doped Ce⁴⁺ ions inhibited grain growth of SrTiO₃.

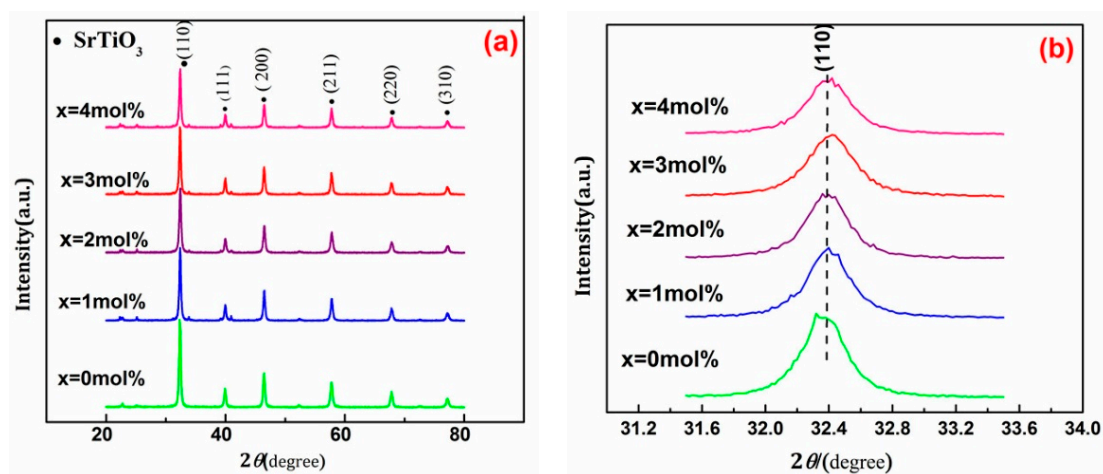


Figure 6. XRD pattern of pure and 1 mol %, 2 mol %, 3 mol %, 4 mol % Ce⁴⁺ doped SrTiO₃. (a) The whole XRD pattern; (b) The local enlargement of the diffraction peaks at 2θ = 32.4°.

The average particle size of samples was calculated by the Debye-Scherrer formula. The average particle size of SrTiO₃ samples with the doping amount of Ce⁴⁺ 0~4 mol % were 20.8 nm, 17.2 nm, 13.3 nm, 8.7 nm, and 18.7 nm, respectively. Additionally, compared with pure SrTiO₃, the specific surface area and pore volume of Ce⁴⁺ doped SrTiO₃ samples manifestly increased (See Table 3). The specific surface area of 3 mol % Ce⁴⁺ doped SrTiO₃ was more than four times higher than that of pure SrTiO₃.

Table 3. Specific surface area, pore volume, and average pore diameter of the samples.

Catalysts	Surface Area/(m ² ·g ⁻¹)	Pore Volume/(cm ³ ·g ⁻¹)	Mean Pore Size/nm
SrTiO ₃	11.8	0.040	13.6
1 mol % Ce ⁴⁺ doped SrTiO ₃	13.5	0.047	14.2
2 mol % Ce ⁴⁺ doped SrTiO ₃	25.9	0.052	8.1
3 mol % Ce ⁴⁺ doped SrTiO ₃	48.7	0.132	7.7
4 mol % Ce ⁴⁺ doped SrTiO ₃	12.7	0.048	15.2

Sr²⁺ radius was relatively large, leading to relatively large lattice parameters for a SrTiO₃ crystal system. Ti⁴⁺ in the oxygen octahedron system had a good mobility and an inferior stability, which facilitated the fracture of Ti–O bonds. Concurrently, Ti⁴⁺ produced a positive charge at the grain boundary. The replacement of Sr²⁺ by Ce⁴⁺ with a smaller radius engendered volume contraction of the unit cell. Thus, the activity scope of Ti⁴⁺ ion was smaller, and additional Ti–O bonds were not easily broken [13,14], leading to a reduction in the positive charge of the grain boundary. Space contraction was generated, leading to the decrease in grain size and further increasing the specific surface area. However, the grain size of SrTiO₃ did not continue to decrease with the increase in the content of Ce⁴⁺. Compared with 3 mol % Ce⁴⁺ doped SrTiO₃, the average particle size of 4mol% Ce⁴⁺ doped SrTiO₃ slightly increased. When an excess of Ce⁴⁺ gathered on the surface of SrTiO₃, a positive charge on the boundary surface increased and space area expanded. Thus, while the crystal grain increased the specific surface area decreased.

Figure 7 displays the FTIR curves of the samples. FTIR curves of the differing amounts of Ce⁴⁺ doped SrTiO₃ all exhibited the characteristic absorption peak of hydroxyl vibration at 3420 cm⁻¹ and 1629 cm⁻¹ [15]. It is suggested that the hydroxyl group stemmed from the adsorbed water on the surface of the samples. The absorption peaks at 557 cm⁻¹ were attributed to the stretching vibration of the Sr–Ti–O bond [14]. No additional peaks appeared at this wavelength range for Ce⁴⁺ doped SrTiO₃. The characteristic absorption peak at 1145 cm⁻¹ for CeO₂ was not observed, evincing that doped Ce⁴⁺ entered into the crystal lattice of SrTiO₃. According to the XRD test results, the Ti–O bond length shortened after the substitution of Ce⁴⁺ for Sr²⁺, and the absorption peak of Ti–O bond widened due to the presence of several with a Sr–Ti–O absorption peak.

Figure 8 shows the XPS spectra. Figure 8a reveals that the Ce⁴⁺ was not detected in the 3 mol % Ce⁴⁺ doped SrTiO₃, indicating that the Ce⁴⁺ was indeed highly dispersed in the bulk phase of SrTiO₃, which is in accordance with the above analysis. Through quantitative analysis (Table 4), n (Sr) / n (Ti) in pristine SrTiO₃ system was 0.96, possibly signifying the excess Ti⁴⁺ distributed on the crystal surface. The content of Ti⁴⁺ decreased from 13.77% to 13.01% after 3 mol % Ce⁴⁺ doping, also indicating that the reduction of the content of the crystal surface of Ti⁴⁺ was attributable to the substitution of Ce⁴⁺ for Sr²⁺. Simultaneously, the O content on the surface of SrTiO₃ increased. The O_{1s} peak was fitted. The SrTiO₃ of pure O_{1s} can be divided into three peaks at 529.28, 530.73, and 532.55 eV [8,16,17], respectively, as shown in Figure 8b marked “1”, “2” and “3”. The “1” peak belonged to the characteristic peak of lattice oxygen, and the “2” peak was born of the adsorbed oxygen on the surface. “3” corresponded to the characteristic peak of the physisorption water on the sample surface.

After doping, three peaks for O_{1s} shifted 0.01 eV, 0.35 eV, and 0.31 eV to higher binding energy sites. The smaller atomic radius, the larger both the electronegativity and electron binding energy is. The Ce electronegativity of 1.12 was more than that of Sr (0.95). After the Ce⁴⁺ replaced Sr²⁺,

the electron density around Sr and Ti decreased, the shielding effect was weakened, and the electron binding energy increased.

A comparison of Figure 8b and 8c demonstrates that the intensity of “2” and “3” peaks increased after doping. The surface oxygen adsorption increased from 26.55% to 28.74% by calculating the area of three peaks. The physical adsorption of H₂O O_{1s} increased from 17.74% to 20.8%, which was attributed to an increased specific surface area of doped Ce⁴⁺ as well as enhanced adsorption capacity.

Some adsorbed oxygen were able to capture some free electrons on the surface of SrTiO₃ to form the active center in the catalytic reaction process. The higher the adsorbed oxygen content on the surface of SrTiO₃, the higher the catalytic activity was.

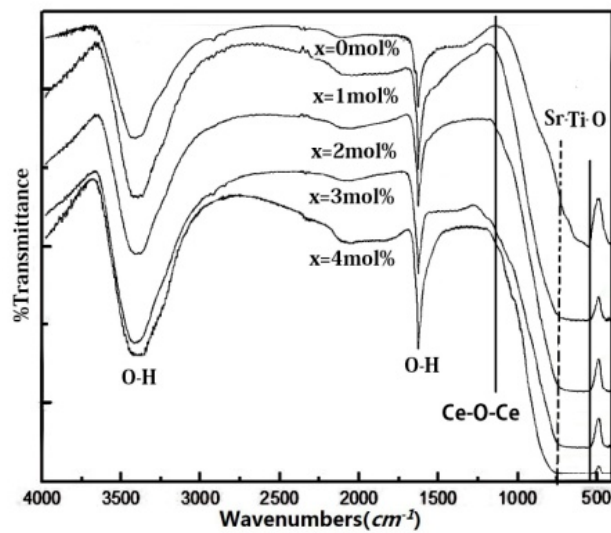


Figure 7. FTIR spectra of pure SrTiO₃ and 1 mol %, 2 mol %, 3 mol %, 4 mol % Ce⁴⁺ doped SrTiO₃.

Table 4. Surface atomic composition and atomic ratio of catalysts.

Catalysts	Surface Atomic Composition			Surface Atomic Ratio
	Sr	Ti	O	n(Sr)/n(Ti)
SrTiO ₃	24.18%	13.77%	55.44%	0.96
3 mol %Ce ⁴⁺ doped SrTiO ₃	25.02%	13.01%	57.19%	1.05

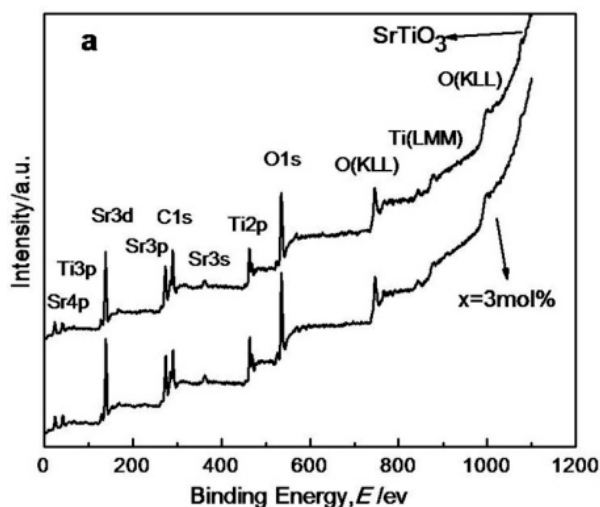


Figure 8. Cont.

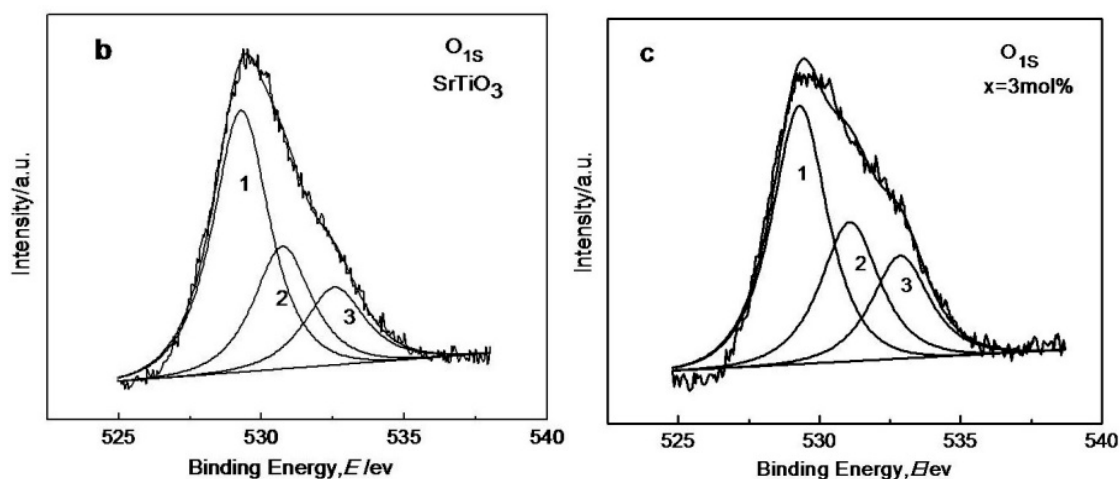


Figure 8. XPS scans for pure and 3 mol % Ce^{4+} doped SrTiO_3 (a) Full scan; (b) O_{1s} peaks on pure SrTiO_3 ; (c) O_{1s} peaks on 3 mol % Ce^{4+} doped SrTiO_3 .

Analysis of the SEM image (See Figure 9) were consistent with those of XRD and BET. It can be seen from Figure 5 that pure SrTiO_3 particles were spherical. The observed partial agglomeration was due to the volatilization or decomposition of organic material during the roasting process. However, 3 mol % Ce^{4+} doped SrTiO_3 particles were smaller and had uniform distribution. The agglomeration significantly could be ameliorated.

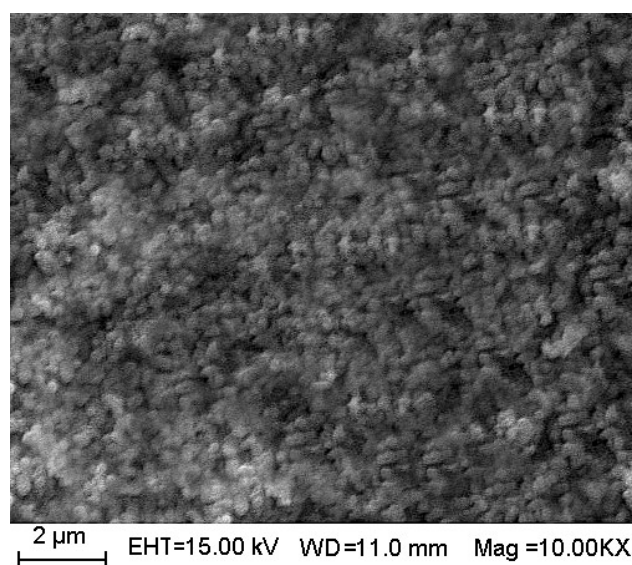


Figure 9. SEM images of 3 mol % Ce^{4+} doped SrTiO_3 .

3.4. Optical Properties and Photocatalytic Activity

Figure 10 was the UV-Vis diffuse reflectance spectra of pure SrTiO_3 and Ce^{4+} doped SrTiO_3 catalysts. It can be seen from Figure 10 that the absorption light region for pure SrTiO_3 was only in the ultraviolet light range. However, Ce^{4+} doped SrTiO_3 in 500 nm wavelength produced an observable characteristic absorption peak. The absorption peak could be ascribable to electronic transitions of Ce^{4+} [8]. This further proved that Ce^{4+} had entered into the crystal lattice of SrTiO_3 . In the range of 1–3 mol %, the absorbance intensity gradually increased.

The absorbance of 4 mol % Ce doped SrTiO₃ in the visible region increased significantly compared with SrTiO₃. The absorbance of 4 mol% Ce doped SrTiO₃ in the visible light range was lower than that of 1–3 mol % doping amount. This was attributable to the change of the content of each element and the surface morphology. The results were in conformity with those of XRD BET and SEM tests.

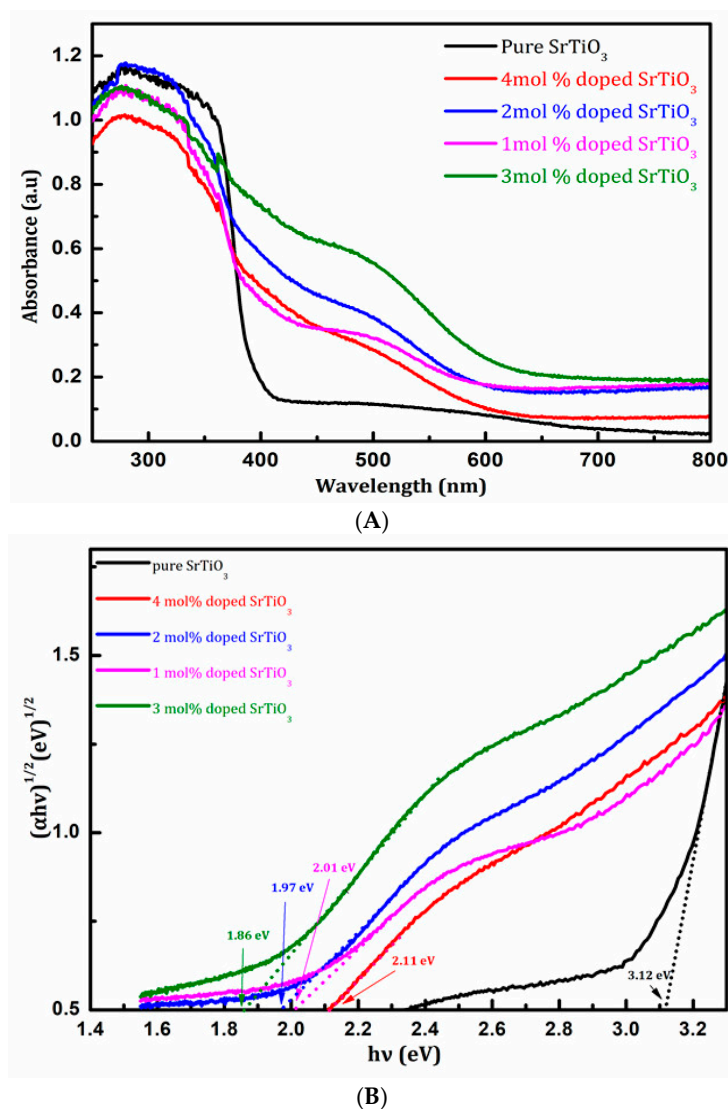


Figure 10. (A) UV-vis diffuse reflectance spectra of samples; (B) The plot of $(\alpha h\nu)^2$ vs. $h\nu$ to estimate the E_g value. (black) pure SrTiO₃; (purple) 1 mol % Ce⁴⁺ doped SrTiO₃; (blue) 2 mol % Ce⁴⁺ doped SrTiO₃; (green) 3 mol % Ce⁴⁺ doped SrTiO₃; (red) 4 mol % Ce⁴⁺ doped SrTiO₃.

3.5. Photocatalytic Activity and Corresponding Mechanism

3.5.1. Effect of Initial Concentration of Methylene Blue on Photocatalytic Activity

It can be seen from Table 5 that the degradation efficiency of 100 mg/L MB after 2 h reaction using 3 mol % Ce doped SrTiO₃ under visible light irradiation reached 45.4% which was the highest degradation efficiency (See Figure 11).

Table 5. Effect of initial concentration on photocatalytic activity.

Samples	Degradation Efficiency (%)				
	20 mg/L	50 mg/L	100 mg/L	150 mg/L	200 mg/L
SrTiO ₃	3.8	4.7	6.1	5.6	4.5
1 mol % Ce ⁴⁺ doped SrTiO ₃	10.1	15.5	18.6	17.2	15.6
2 mol % Ce ⁴⁺ doped SrTiO ₃	12.7	21.8	31.4	29.6	23.1
3 mol % Ce ⁴⁺ doped SrTiO ₃	27.2	36.2	45.4	39.4	35.4
4 mol % Ce ⁴⁺ doped SrTiO ₃	4.3	8.7	12.4	9.7	7.6

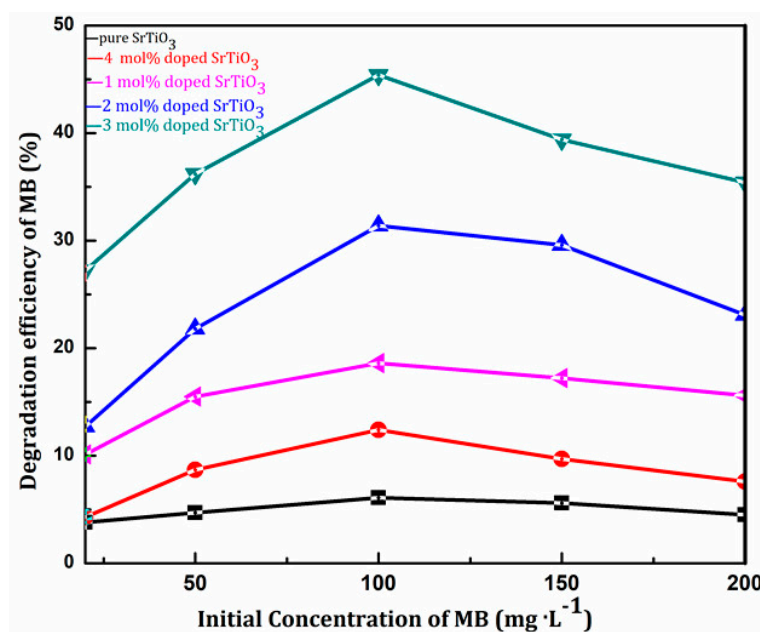


Figure 11. Effect of initial concentration on photocatalytic activity. (black) pure SrTiO₃; (purple) 1 mol % Ce⁴⁺ doped SrTiO₃; (blue) 2 mol % Ce⁴⁺ doped SrTiO₃; (green) 3 mol % Ce⁴⁺ doped SrTiO₃; (red) 4 mol % Ce⁴⁺ doped SrTiO₃.

The lower the initial concentration of methylene blue, the lighter the color was. Thus, the light source had a strong penetrating ability in the solution. However, a lower initial concentration resulted in making concentration diffusion the rate-controlling step in the whole photocatalytic kinetics. In such an occurrence, photocatalytic effect decreased.

However, when the MB concentration was greater than 100 mg/L, the solution color was darker, which significantly obstructed the absorption to visible light and further affected the optimal degradation action. Therefore, the concentration of methylene blue (100 mg/L) was chosen to investigate the photocatalytic activity for the subsequent test.

3.5.2. Photocatalytic Activity and Mechanism

From Figure 12, we can observe the maximum degradation efficiency of methylene blue for pure SrTiO₃ was only 40%. The photocatalytic activity gradually increased with the increase in doped Ce⁴⁺ content. The degradation efficiency of methylene blue could reach to 98.7% using 3 mol % Ce⁴⁺ doped SrTiO₃.

(1) According to the photocatalytic mechanism of SrTiO₃ (Figure 12), under light irradiation, the photogenerated electron and hole separated and moved to different locations on the particle surface to participate redox reactions for organic compounds degradation. The recombination of the photogenerated electron and hole was one of the reasons for the low photocatalytic efficiency of

SrTiO₃. XRD, BET and SEM tests indicated that as the average particle size of Ce⁴⁺ doped SrTiO₃ decreased, the specific surface area increased. The photo-excited electron and hole needed to migrate to the surface to play the catalytic role. The smaller the particle size, the shorter migration distance was [18]. Accordingly, the recombination possibility of the photo-excited electron and hole became smaller. In addition, the Ce⁴⁺ doping improved agglomeration. The surface of the catalyst active center was able to absorb ultraviolet light irradiation [19] which enhanced photocatalytic performance.

(2) Figure 13 shows that the adsorption oxygen on the surface of SrTiO₃ quickly captured electrons to inhibit recombination of photo-excited electron and hole. Meanwhile, it also could adsorb oxygen and H₂O to produce ·OH and h⁺. The photo-excited hole could directly transform the surface adsorption of H₂O into ·OH, which was the active center [20,21]. From the analysis of XPS, Ce⁴⁺ doping increased the amount of surface adsorption of oxygen and H₂O. Thus, Ce⁴⁺ doped SrTiO₃ could produce more ·OH to enhance photocatalytic ability.

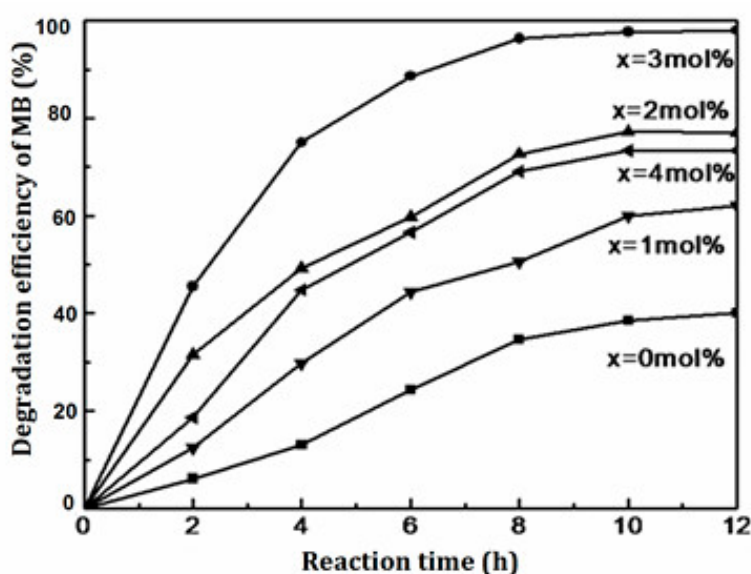


Figure 12. The photocatalytic degradation on MB of 0~4 mol % Ce⁴⁺ doped SrTiO₃.

(3) In addition, the UV-vis diffuse reflectance spectrum demonstrated that the band gap width of 3 mol % Ce⁴⁺ doped SrTiO₃ became smaller (See Figure 10). This was because the Ce⁴⁺ doping could introduce the 4f orbital energy level into the mid-st band gap of SrTiO₃. On the one side, this reduced the band gap of SrTiO₃, which made the excitation wavelength of SrTiO₃ shift from the ultraviolet light range to the visible light range, boosting the utilization rate of visible light. On the other side, this created new energy states, namely, mid-gap states, that facilitated the photo-excited electron to jump into the conduction band and to achieve effective separation between the photo-excited electron and the hole. In other words, the doping of Ce⁴⁺ could create new energy states that could delay the exciton recombination time and could allow charge separation.

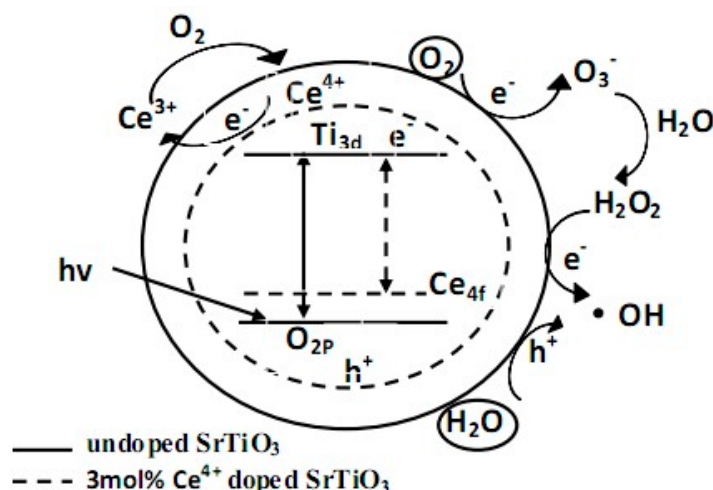


Figure 13. Schematic diagram of photocatalytic mechanism.

(4) Furthermore, the reduction potential of Ce⁴⁺/Ce³⁺ was 1.61 eV. Ce⁴⁺ on 4f energy level easily captured electrons to generate Ce³⁺. The generated Ce³⁺ in turn could be oxidized to Ce⁴⁺ by oxygen on the catalyst surface or in the air [22]. The photoexcited electron was captured continuously by Ce⁴⁺, which further inhibited the recombination between the photo-excited electron and the hole.

In comparison to 3 mol % Ce⁴⁺ doped SrTiO₃, photocatalytic activity of 4 mol % Ce⁴⁺ doped SrTiO₃ decreased. An excessively doped Ce⁴⁺ increased the size of the catalyst particle size. Moreover, n(Sr)/n(Ti) in the Ce⁴⁺ doped SrTiO₃ increased (See Table 4), indicating that excessive doping brought out the generation of SrO on the surface of SrTiO₃, which impeded the light absorption for SrTiO₃ and affected its catalytic activity.

4. Conclusions

(1) The tartaric acid aqueous solution is used as a solvent, dispersant, and stabilizer to prepare SrTiO₃ using the sol-gel method. The improved preparation method has some advantages, for example, the simplicity of the process with less equipment, its short preparation time, and its low cost. When 1.47 g SrCO₃ was weighted to synthesize SrTiO₃, the optimum molar ratio of Sr²⁺ and tartaric acid was 1:4. The optimum amount of distilled water was 20 mL. In practical application, we can adjust the molar ratio (Sr²⁺—tartaric acid) and the amount of water on the basis of the quality of SrCO₃.

(2) The degradation efficiency of methylene blue reached 98.7% using 3 mol % Ce⁴⁺ doped SrTiO₃, indicating it had an excellent photocatalytic activity. The introduction of Ce⁴⁺ into the SrTiO₃ revealed several prominent advantages: (i) The Ce⁴⁺ doping increased specific surface area more than four times compared with pure SrTiO₃; (ii) The doped Ce⁴⁺ enhanced the physical adsorption of H₂O and adsorbed oxygen on the surface of SrTiO₃ to produce more catalytic active centers; (iii) The incorporation of Ce⁴⁺ into the crystal lattice for SrTiO₃ created mid-gap states that delay the exciton recombination time and allow for charge separation; (iv) Ce⁴⁺ repeatedly captured photoelectron to produce Ce³⁺, which inhibited the recombination of photogenerated electrons and holes.

Acknowledgments: We want to thank the financial support from Youth research talents' growth support program of Yangtze Normal University and Chongqing Basic Science and Advanced Technology Research Program (CSTC2015jcyjBX0015). We gratefully acknowledge many important contributions from the researchers of all reports cited in our paper.

Author Contributions: Taiping Xie and Longjun Xu conceived and designed the experiments; Yuan Wang performed the experiments; Yuan wang and Taiping Xie analyzed the data; Chenglun Liu contributed reagents/materials/analysis tools; Taiping Xie and Yuan wang wrote the paper.

Conflicts of Interest: The authors declare that they have no conflict of interest.

References

1. Cao, T.P.; Li, Y.J.; Wang, C.H.; Shao, C.L.; Liu, Y.C. A Facile in Situ Hydrothermal Method to SrTiO₃/TiO₂ Nanofiber Heterostructures with High Photocatalytic Activity. *Langmuir* **2011**, *27*, 2946–2952. [[CrossRef](#)] [[PubMed](#)]
2. Mao, M.Y.; Li, Y.Z.; Hou, J.T.; Zeng, M.; Zhao, X.J. Extremely efficient full solar spectrum light driven thermocatalytic activity for the oxidation of VOCs on OMS-2 nanorod catalyst. *Appl. Catal. B* **2015**, *174*, 496–503. [[CrossRef](#)]
3. Xie, T.P.; Xu, L.J.; Liu, C.L. Magnetic composite BiOCl-SrFe₁₂O₁₉: A novel p-n type heterojunction with its enhanced photocatalytic activity. *Dalton Trans.* **2014**, *43*, 2211–2220. [[CrossRef](#)] [[PubMed](#)]
4. Navarro, R.M.; Alvarez-Galvan, M.C.; de la Mano, J.A.V. A framework for visible-light water splitting. *Energy Environ. Sci.* **2010**, *3*, 1865–1882. [[CrossRef](#)]
5. Wang, L.; Ji, Z.Y.; Lin, J.J.; Li, P. Preparation and optical and photocatalytic properties of Ce-doped ZnO microstructures by simple solution method. *Mater. Sci. Semicon. Proc.* **2017**, *71*, 401–408. [[CrossRef](#)]
6. Rezaei, M.; Habibi-Yangjeh, A. Simple and large scale refluxing method for preparation of Ce-doped ZnO nanostructures as highly efficient photocatalyst. *Appl. Surf. Sci.* **2013**, *265*, 591–596. [[CrossRef](#)]
7. Adel, M.F.; Ahmed, A.I.; Ibrahim, A.; Bouzid, H.; Al-Sayari, S.A. Highly efficient photocatalyst based on Ce doped ZnO nanorods: Controllable synthesis and enhanced photocatalytic activity. *Chem. Eng. J.* **2013**, *229*, 225–233.
8. Piña-Pérez, Y.; Tzompantzi-Morales, F.; Pérez-Hernández, R.; Arroyo-Murillo, R.; Acevedo-Peña, P.; Gómez-Romero, R. Photocatalytic activity of Al₂O₃ improved by the addition of Ce³⁺/Ce⁴⁺ synthesized by the sol-gel method. Photodegradation of phenolic compounds using UV light. *Fuel* **2017**, *198*, 11–21. [[CrossRef](#)]
9. Bharatvaj, J.; Preethi, V.; Kanmani, S. Hydrogen production from sulphide wastewater using Ce³⁺ TiO₂ photocatalysis. *Int. J. Hydrogen Energy* **2018**, *43*, 3935–3945. [[CrossRef](#)]
10. Ong, C.B.; Ng, L.Y.; Mohammad, A.W. A review of ZnO nanoparticles as solar photocatalysts: Synthesis, mechanisms and applications. *Renew. Sust. Energy Rev.* **2018**, *81*, 536–551. [[CrossRef](#)]
11. Hou, D.F.; Hu, X.L.; Ho, W.K.; Hu, P.; Huang, Y.H. Facile fabrication of porous Cr-doped SrTiO₃ nanotubes by electrospinning and their enhanced visible-light-driven photocatalytic properties. *J. Mater. Chem. A* **2015**, *3*, 3935–3943. [[CrossRef](#)]
12. Lehuta, K.A.; Kittilstved, K.R. Speciation of Cr(III) in intermediate phases during the sol-gel processing of Cr-doped SrTiO₃ powders. *J. Mater. Chem. A* **2014**, *2*, 6138–6145. [[CrossRef](#)]
13. Canu, G.; Buscaglia, V. Hydrothermal synthesis of strontium titanate: Thermodynamic considerations, morphology control and crystallisation mechanisms. *Cryst. Eng. Comm.* **2017**, *19*, 3867–3891. [[CrossRef](#)]
14. Ha, M.N.; Zhu, F.; Liu, Z.; Wang, L.; Liu, L.; LU, G.; Zhao, Z. Morphology-Controlled Synthesis SrTiO₃/TiO₂ Heterostructures and Their Photocatalytic Performance for Water Splitting. *RSC Adv.* **2016**, *6*, 21111–21118. [[CrossRef](#)]
15. Xie, T.P.; Liu, C.L.; Xu, L.J. Novel heterojunction Bi₂O₃/SrFe₁₂O₁₉ magnetic photocatalyst with highly enhanced photocatalytic activity. *J. Phys. Chem. C* **2013**, *117*, 24601–24610. [[CrossRef](#)]
16. Liu, F.M.; Xie, Y.; Yu, C.L.; Liu, X.M.; Dai, Y.H.; Liu, L.J. Novel hybrid Sr-doped TiO₂/magnetic Ni_{0.6}Zn_{0.4}Fe₂O₄ for enhanced separation and photodegradation of organics under visible light. *RSC Adv.* **2015**, *5*, 24056–24063. [[CrossRef](#)]
17. Kutty, T.R.N.; Nag, A. Role of interface states associated with transitional nanophase precipitates in the photoluminescence enhancement of SrTiO₃:Pr³⁺, Al³⁺. *J. Mater. Chem.* **2003**, *13*, 2271–2278. [[CrossRef](#)]
18. Saadetnejad, D.; Yildirim, R. Photocatalytic hydrogen production by water splitting over Au/Al-SrTiO₃. *Int. J. Hydrogen Energy* **2018**, *43*, 1116–1122. [[CrossRef](#)]
19. Shah, Z.H.; Ge, Y.Z.; Ye, W.Y. Visible light activation of SrTiO₃ by loading Ag/AgX (X = Cl, Br) for highly efficient plasmon-enhanced photocatalysis. *Mater. Chem. Phys.* **2017**, *198*, 73–82. [[CrossRef](#)]
20. Wang, C.D.; Qiu, H.; Inoue, T.; Yao, Q.W. Band gap engineering of SrTiO₃ for water splitting under visible light irradiation. *Int. J. Hydrogen Energy* **2014**, *39*, 12507–12514. [[CrossRef](#)]

21. Sakata, Y.; Miyoshi, Y.; Maeda, T.; Ishikiriyama, K. Photocatalytic property of metal ion added SrTiO₃ to Overall H₂O splitting. *Appl. Catal. A* **2016**, *521*, 227–232. [[CrossRef](#)]
22. Dong, B.; Lia, L.Y.; Dong, Z.F.; Xu, R.; Wu, Y. Fabrication of CeO₂ nanorods for enhanced solar photocatalysts. *Int. J. Hydrogen Energy* **2018**, *43*, 5275–5282. [[CrossRef](#)]



© 2018 by the authors. Licensee MDPI, Basel, Switzerland. This article is an open access article distributed under the terms and conditions of the Creative Commons Attribution (CC BY) license (<http://creativecommons.org/licenses/by/4.0/>).